Molecular Therapy
Nucleic Acids
Original Article

miR-379 mediates insulin resistance and obesity through impaired angiogenesis and adipogenesis regulated by ER stress

Maryam Abdollahi,[1] Mitsuo Kato,[1] Linda Lanting,[1] Ragadeepthi Tunduguru,[1] Mei Wang,[1] Yangmeng Wang,[1] Patrick T. Fueger,[2,3] Qiong Wang,[2] Wendong Huang,[1] and Rama Natarajan[1]

[1]Department of Diabetes Complications and Metabolism, Arthur Riggs Diabetes and Metabolism Research Institute, Beckman Research Institute of City of Hope, Duarte, CA 91010, USA; [2]Department of Molecular and Cellular Endocrinology, Arthur Riggs Diabetes and Metabolism Research Institute, Beckman Research Institute of City of Hope, Duarte, CA 91010, USA; [3]Comprehensive Metabolic Phenotyping Core, Beckman Research Institute of City of Hope, Duarte, CA 91010, USA

We investigated the role of microRNA (miR-379) in the pathogenesis of obesity, adipose tissue dysfunction, and insulin resistance (IR). We used miR-379 knockout (miR-379KO) mice to test whether loss of miR-379 affects high-fat diet (HFD)-induced obesity and IR via dysregulation of key miR-379 targets in adipose tissue. Increases in body weight, hyperinsulinemia, and IR in wild-type (WT)-HFD mice were significantly attenuated in miR-379KO-HFD mice with some sex differences. Relative to control chow-fed mice, in WT-HFD mice, expression of miR-379 and C/EBP homologous protein (*Chop*) (pro-endoplasmic reticulum [ER] stress) and inflammation in perigonadal white adipose tissue (gWAT) were increased, whereas adipogenic genes and miR-379 target genes (*Vegfb* and *Edem3*) were decreased. These changes, as well as key parameters of brown adipose tissue dysfunction (including mitochondrial defects), were significantly attenuated in miR-379KO-HFD mice. WAT from obese human subjects with and without type 2 diabetes showed increased miR-379 and decreased miR-379 target genes. In cultured 3T3L1 pre-adipocytes, miR-379 inhibitors increased miR-379 targets and adipogenic genes. These data suggest that miR-379 plays an important role in HFD-induced obesity through increased adipose inflammation, mitochondrial dysfunction, and ER stress as well as impaired adipogenesis and angiogenesis. miR-379 inhibitors may be developed as novel therapies for obesity and associated complications.

INTRODUCTION

Obesity is a highly prevalent metabolic disorder and a significant healthcare challenge worldwide.[1] Obesity and associated inflammation increase the risk of insulin resistance (IR), type 2 diabetes (T2D), and vascular disorders.[2] Although lifestyle and diet modifications prevent and correct obesity, in practice, adherence to such programs is often suboptimal.

Adipose tissue is composed of many cell types, including adipocytes, macrophages, and endothelial cells, which, in certain situations, may contribute to chronic inflammation, oxidative stress,[3] and impaired angiogenesis,[4] resulting in adipose tissue expansion and dysfunction. Intake of a high-fat diet (HFD) promotes local infiltration of immune cells, such as macrophages, into white adipose tissue and increases inflammation and IR.[5] Such changes are closely linked to visceral adipose tissue dysfunction, T2D, and cardiovascular disease.[6]

Non-coding RNAs (ncRNAs) represent an additional layer of gene regulation. There is growing interest in the mechanistic role played by ncRNAs (including long ncRNAs [lncRNAs] and microRNAs [miRNAs]) and their specific gene targets in various human disorders. lncRNAs are long transcripts (>200 nt) similar to messenger RNAs (mRNAs) but lack protein-coding (translation) potential.[7] lncRNAs regulate the expression of local and distal genes by various mechanisms that include recruitment of histone-modifying complexes, RNA-binding proteins, and modulation of transcription factors (TFs).[8] lncRNAs also serve as host genes or sponges for miRNAs (~22 nt). miRNAs participate in post-transcriptional regulation of genes by repressing translation or inducing degradation of target mRNAs, altering cellular functions and disease states.[8,9] lncRNAs and miRNAs are emerging as critical players in diabetes and its complications.[8–11]

We have previously demonstrated a role of key miRNAs and lncRNAs in the pathogenesis of diabetic kidney disease (DKD), inflammation, and vascular disease.[10,12–14] Among these, miR-379 is part of a miRNA cluster within the DLK-DIO3 genomic region (mouse chromosome 12 [chr12], human chr14), which encompasses

Received 28 April 2022; accepted 15 September 2022;
https://doi.org/10.1016/j.omtn.2022.09.015.

Correspondence: Maryam Abdollahi, Department of Diabetes Complications and Metabolism, Arthur Riggs Diabetes and Metabolism Research Institute, Beckman Research Institute of City of Hope, 1500 E. Duarte Road, Duarte, CA 91010, USA.
E-mail: mabdollahi@coh.org
Correspondence: Rama Natarajan, Department of Diabetes Complications and Metabolism, Arthur Riggs Diabetes and Metabolism Research Institute, Beckman Research Institute of City of Hope, 1500 E. Duarte Road, Duarte, CA 91010, USA.
E-mail: rnatarajan@coh.org

multiple miRNAs and lncRNAs.[14,15] We have shown previously that miR-379 and its host transcript lncRNA megacluster, lncMGC, were regulated by the endoplasmic reticulum (ER) stress related TF C/EBP homologous protein (CHOP) and increased in the renal glomeruli of diabetic mice.[14] Genetic deletion of miR-379 ameliorated early DKD in diabetic mice by decreasing ER and oxidative stress and mitochondrial dysfunction. One of the targets of miR-379 with protective functions in the kidney is mitochondrial fission 1 protein (FIS1), which mediates adaptive mitophagy.[15] However, the role of miR-379 in adipose tissue and HFD-induced obesity and IR is unknown.

To determine the *in vivo* functions of miR-379 in these metabolic disorders, we used miR-379^{em1COH} knockout (miR-379KO) mice generated by CRISPR-Cas9 editing.[15] We found control wild-type (WT) mice on a high-fat diet (HFD) showed increased body weight, miR-379 expression in perigonadal white adipose tissue (gWAT), adipocyte hypertrophy, impaired adipogenesis, and IR, as expected. However, such changes were significantly reduced in miR-379KO mice on an HFD with some sex differences. This protection was associated with altered expression of miR-379 target genes implicated in angiogenesis and ER stress as well as genes related to adipogenesis in gWAT, along with reduced inflammation and IR. We also observed improvement in parameters of mitochondrial function in brown adipose tissue (BAT) of miR-379KO-HFD mice. We also found increases in miR-379 and decreases in miR-379 target genes in adipose tissue from obese individuals with and without T2D, demonstrating human relevance. Our data suggest that adipose tissue miR-379 plays a key role in the pathology of obesity and could serve as a potential therapeutic target.

RESULTS

HFD-induced obesity and adipocyte hypertrophy are attenuated in miR-379KO mice

To determine the *in vivo* regulatory effect of miR-379 on obesity, we compared WT and miR-379KO (male [M] and female [F]) mice on an HFD or standard chow diet for 10 and 24 weeks (Figure S1). The mouse lncMGC region hosts the miR-379 megacluster of miRNAs, within which miR-379 is the most 5′ miRNA (Figure S2A). We confirmed a significant reduction of miR-379 in gWAT of miR-379KO mice compared with WT mice (Figure S2B). Body weight was measured weekly up to 10 (Figures S3A and S3B) and 24 weeks of HFD feeding (Figures S3C and S3D) for M and F mice. At 24 weeks, all mice had similar and normal blood glucose levels (BGLs) regardless of sex or genotype (Figures S3E and S3F).

Although WT and miR-379KO mice gained weight on the HFD, miR-379KO-HFD mice clearly appeared less obese than WT-HFD-M mice at 24 weeks (Figure 1A). Consistent with this, average body weight and fat were significantly higher in WT-HFD mice compared with their respective controls, but miR-379KO-HFD-M mice exhibited significantly less weight gain (Figure 1B) and body fat (Figure 1C) than WT-HFD-M mice at 10 and 24 weeks. F miR-379KO mice showed similar phenotypes (Figures 1A, 1D, and 1E). Fat tissue expansion can manifest as increased adipocyte hypertrophy and size.[16] We observed significantly larger adipocytes (hypertrophy) in WT-HFD-M (Figures 1F and 1G) and WT-HFD-F (Figures 1F and 1H) mice, which was significantly attenuated in miR-379KO-HFD-M and -F mice compared with the respective controls at 10 and 24 weeks (Figures 1F–1H). These results show that the increased body weight and adipocyte hypertrophy observed in WT-HFD-M and -F mice are significantly attenuated in miR-379KO-HFD (M and F) mice.

miR-379KO-HFD mice show improved insulin sensitivity

We next measured insulin sensitivity using insulin tolerance tests (ITTs). WT-HFD-M (Figures 2A and 2B) and WT-HFD-F (Figures 2C and 2D) mice exhibited significant IR compared with controls, as expected. In contrast, miR-379KO (M and F) mice showed higher insulin sensitivity after 10 (Figures 2A and 2C) and 24 weeks on the HFD (Figures 2B and 2D). We calculated the area under the curve (AUC) for ITTs at 10 and 24 weeks of HFD feeding. As shown in Figures S4A and S4B, in M mice, the AUC was significantly increased in WT-HFD-M mice at 10 and 24 weeks of HFD feeding compared with WT-control (Con)-M mice. This increase was significantly lower in miR-379KO-HFD-M mice at 10 weeks of HFD feeding. In F mice, the AUC was significantly increased in WT-HFD-F mice and showed significant improvement in miR-379KO-HFD-F mice at 10 and 24 weeks of HFD feeding (Figure S4C and S4D). Plasma insulin levels were increased in WT-HFD-M and WT-HFD-F mice (Figures 2E and 2F), but this was significantly lower in miR-379KO-HFD (M and F) mice. In miR-379KO-F mice, insulin levels after 24 weeks on the HFD were even close to that in mice on the Con chow diet (Figure 2F). We also measured homeostatic model assessment of IR (HOMA-IR) as an index for IR. Increased HOMA-IR values observed in WT-HFD-M (Figure 2G) and WT-HFD-F (Figure 2H) mice were attenuated in miR-379KO-HFD mice (Figures 2G and 2H). miR-379KO-HFD-F mice displayed a higher level of insulin sensitivity compared with miR-379KO-HFD-M mice (Figures 2G and 2H), demonstrating sex-specific differences.

Key metabolic parameters are not significantly different between miR-379KO-HFD and WT-HFD mice

To investigate the mechanisms underlying the protection against weight gain in miR-379KO-HFD mice, we measured key metabolic parameters (Figure S5). As shown in Figure S5, food and water intake were lower in WT-HFD and miR-379KO-HFD (M and F) mice compared with the respective Cons, with no significant differences between WT and miR-379KO mice (Figures S5A, S5B, S5D, and S5E). We measured movement (distance traveled by each mouse) to monitor activity differences. WT-HFD-M and miR-379KO-HFD-M mice showed no differences in mobility relative to their Cons (Figure S5C). WT and miR-379KO HFD-fed F mice displayed reduced movement relative to the respective Con mice (but this was not statistically significant). However, there was no significant difference between WT and miR-379KO-HFD-F mice (Figure S5F). Thus, differences in food intake and movement likely do not contribute to the lower body weight observed in miR-379KO-HFD mice. Using the indirect calorimetry method, we also found no differences in energy

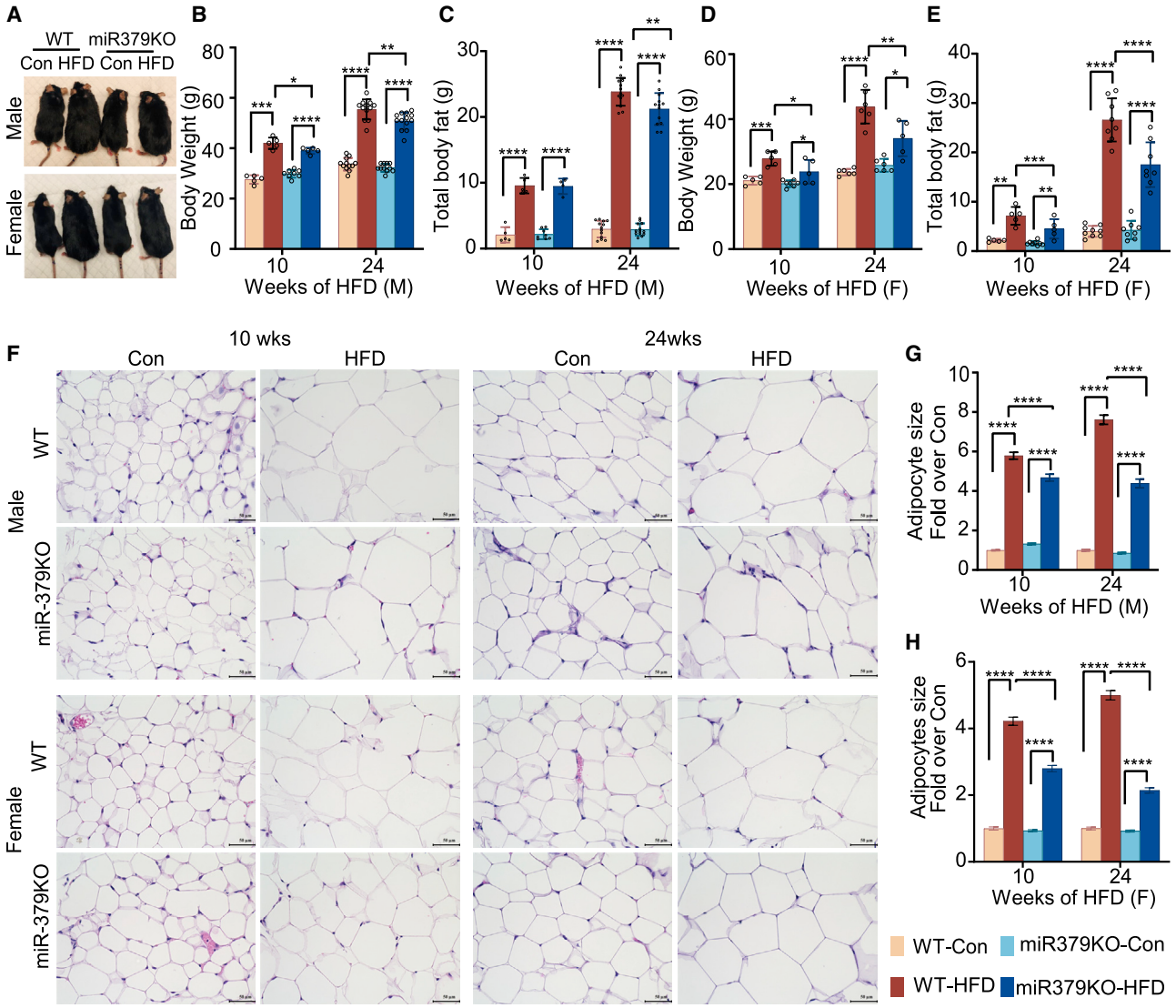

Figure 1. HFD-induced obesity and adipocyte hypertrophy are attenuated in miR-379KO mice

(A) Representative image of male (M) and female (F) WT and miR-379KO control (Con) and HFD-fed mice after 24 weeks on the HFD. (B and D) Average body weight in (B) M and (D) F mice at 10 and 24 weeks of HFD feeding. (C and E) Total body fat in (C) M and (E) F mice. n = 5–8/group for 10 weeks of study and n = 11–14/group for 24 weeks of study in M mice. n = 5–8/group for 10 weeks of study and n = 8–9/group for 24 weeks of study in F mice. Each dot represents one mouse/group. (F) The size of adipocytes in gWAT sections (H&E staining), which are smaller in miR-379 KO-HFD mice versus WT-HFD mice at 10 and 24 weeks on the HFD in M and F mice, respectively. (G and H) Quantitative analysis of adipocyte size in (G) M and (H) F mice. n = 100 adipocytes/group. One-way ANOVA with post hoc Tukey's test for multiple comparisons; ±SEM; *p < 0.05, **p < 0.01, ***p < 0.001, ****p < 0.0001. Scale bars, 50 μm; 40× magnification.

expenditure between the WT-HFD and miR-379KO-HFD groups (data not shown).

Lack of miR-379 is associated with increases in markers of mitochondrial function in BAT

Because we observed no difference in metabolic parameters, we next examined whether there were differences in key BAT parameters, including whitening of BAT and mitochondrial defects between HFD-fed WT and miR-379KO mice, because BAT contains high levels of mitochondria and is specialized for thermogenesis. These effects decline in obesity because of whitening of the BAT.[17] We first examined BAT histology and structure using H&E staining (Figure 3A) and levels of FIS1, a target of miR-379 and key mediator of adaptive mitophagy,[15] (Figure 3B) as well as uncoupling protein-1 (UCP-1), a marker of thermogenesis and mitochondrial function in BAT[18] (Figure 3C), using immunohistochemistry (IHC) staining. The increased whitening of BAT and lipid droplets noted in WT-HFD-M and WT-HFD-F mice relative to the Cons were attenuated

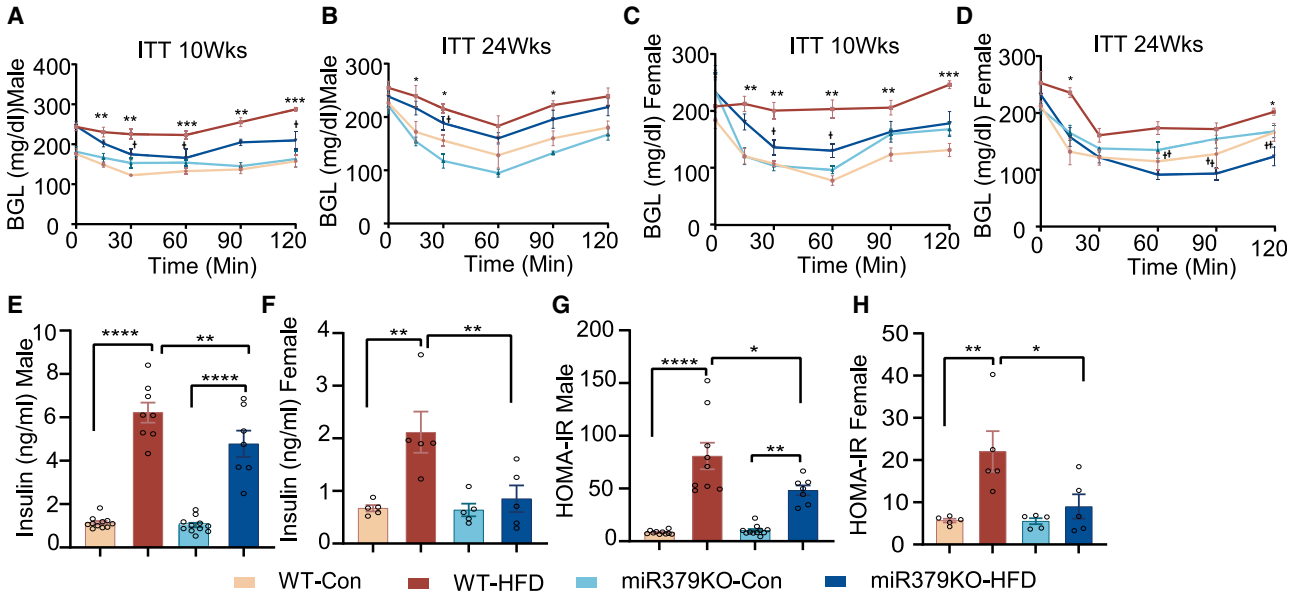

Figure 2. miR-379KO-HFD mice show improved insulin sensitivity

(A and B) Insulin tolerance test (ITT) in M mice after (A) 10 and (B) 24 weeks of HFD feeding. (C and D) ITT in F mice at (C) 10 and (D) 24 weeks of HFD feeding. n = 4–8/group. (E and F) Plasma insulin levels in (E) M and (F) F mice after 24 weeks of HFD feeding. n = 7–11/group for M; n = 5/group for F. (G and H) Homeostatic model assessment of IR (HOMA-IR) in (G) M and (H) F mice. n = 7–11/group for M; n = 5/group for F. Each dot represents one mouse/group. (A–D) *p < 0.05, **p < 0.01, ***p < 0.001 versus WT-Con. $^{+}$p < 0.05, $^{++}$p < 0.01versus WT-HFD, using two-way repeated measures ANOVA. One-way ANOVA with post hoc Tukey's test for multiple comparisons; ±SEM; *p < 0.05, **p < 0.01, ***p < 0.001, ****p < 0.0001.

in miR-379KO-HFD mice (Figure 3A). Expression of FIS1 and UCP-1 was significantly reduced in WT-HFD (M and F) mice relative to WT-Con, and this was significantly restored in miR-379KO-HFD-M and F mice (Figures 3B–3G). Expression of miR-379 was significantly increased in BAT from WT-HFD-M and F mice compared with WT-Con mice (Figures 3H and 3I). Gene expression of *Fis1* and *Ucp-1* was also reduced in BAT from WT-HFD-M mice versus WT-Con but not in the corresponding miR-379KO-HFD-M mice. In miR-379-HFD-F mice, levels of *Fis-1* were higher than in WT-HFD-F mice (Figure 3K). Because some miRNA targets are also regulated at the post-transcriptional/translational level, translation of Fis1 protein in BAT may also be regulated by miR-379. Male UCP-1 gene expression (Figure 3L) and protein expression (Figure 3F) were consistent with each other, but data for female UCP-1 between gene (Figure 3M) and protein level expression (Figure 3G) were not very consistent. The reason for this is not clear and may be due to differences in mRNA or protein stability in F mice.

Next, to strengthen our conclusions related to mitochondrial function, we performed transmission electron microscopy (TEM) examination in BAT from WT and miR-379KO-HFD-fed (M and F) mice. As shown in Figures S6A and S6B, the abnormal mitochondrial structures and disrupted mitochondrial cristae observed in WT-HFD-M and -F mice were attenuated in miR-379KO-HFD-M and -F mice.

We also measured the expression of *Pgc-1α* as a marker of mitochondrial biogenesis in BAT from WT and miR-379KO mice. *Pgc-1α* mRNA expression was significantly reduced in WT-HFD (M and F) mice relative to WT-Con, and this reduction was significantly reversed in miR-379KO-HFD-M and -F mice (Figures S7A and S7B). Next, we measured PGC-1α protein levels using IHC staining. The data in Figure S7C and the bar graph quantifications in Figures S7D and S7E show that, relative to the Cons, PGC-1a levels were significantly decreased in WT-HFD-M and -F mice, and this was restored in miR-379KO-HFD (M and F) mice. These data demonstrate that increases in key parameters of mitochondrial dysfunction in BAT of WT-HFD mice are significantly attenuated in miR-379KO-HFD mice.

Increased expression of miR-379 and *Chop* and decreased expression of adipogenic markers in gWAT of WT-HFD mice are reversed in miR-379KO-HFD mice

We observed increased expression of miR-379 (Figures 4A and 4B) as well as *Chop* (Figures 4C and 4D), which encodes the ER stress-related TF CHOP, in gWAT of WT-HFD (M and F) versus WT-Con mice. These increases were significantly ameliorated in gWAT of miR-379KO-HFD mice (Figures 4C and 4D). Adipose tissue differentiation is an important feature of adipose tissue function and adipogenesis.[19] Therefore, we measured expression of key adipogenic markers. In gWAT from WT-HFD (M and F) mice, *Pparg* (peroxisome proliferator-activated receptor *γ)* expression was decreased (Figures 4E and 4H); however, this was not observed in gWAT from miR-379KO-HFD mice versus the corresponding Cons. C/EBPβ (CCAAT-enhancer-binding protein) expression showed

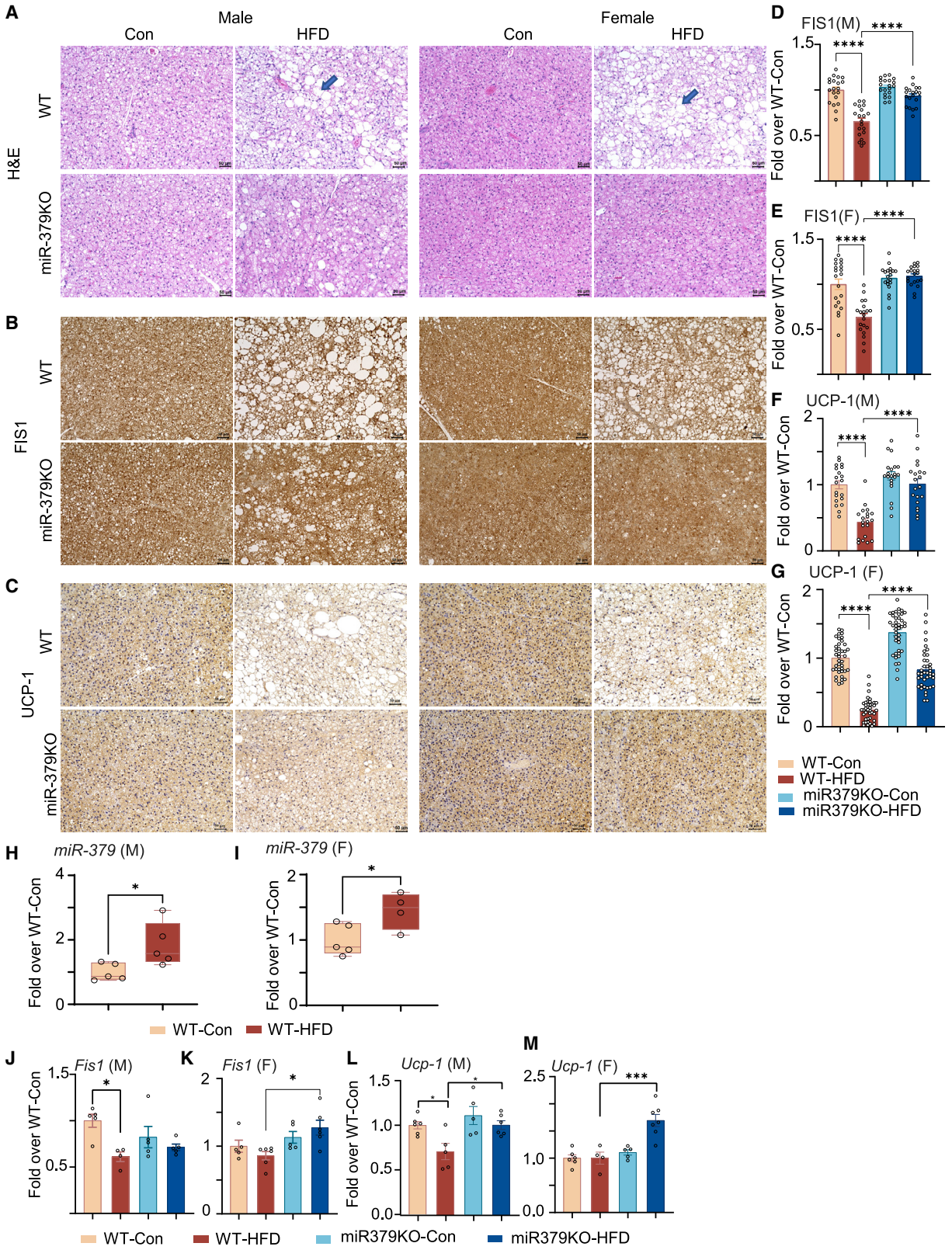

(legend on next page)

similar trends (Figures 4F and 4I). Forkhead-boxO1 (FOXO1) is a downstream target of AKTkinase (Protein kinase B)[20] that also regulates *Pparg* expression.[21] Expression of *FoxO1* was also decreased in gWAT from WT-HFD mice (the decrease in M was not statistically significant), but this decrease was not observed in gWAT from miR-379KO-HFD (M and F) mice (Figures 4G and 4J).

We measured the expression of two other miRNAs in the cluster, miR-411 and miR-494, in gWAT from WT and miR-379KO mice. As shown in Figures S8A–S8D, expression of these miRNAs was not altered between the four groups of mice (M and F).

Decreased expression of miR-379 target genes in gWAT of WT-HFD mice is reversed in miR-379KO-HFD mice

Previously, using the unbiased Argonaute2-CLASH (cross-linking, ligation, sequencing hybrids) approach, we identified key miR-379 targets in mouse kidney mesangial cells, including *Edem3*, *Vegfb*, *Fis1*, and *Txn1*.[15] Vascular endothelial growth factor B (VEGFB) a proangiogenic factor, modulates adipose tissue vascularization.[22] EDEM3 is an ER stress negative regulator,[14] and FIS1 promotes adaptive mitophagy and is important for mitochondrial function.[15] Expression of *Edem3* and *Vegfb* was significantly reduced in gWAT from WT-HFD-M mice (Figure 4K), and that of *Fis1* and *Vegfb* was significantly reduced in gWAT from WT-HFD-F mice (Figure 4L) relative to the corresponding Cons. These reductions were significantly ameliorated (fully or partly) in the corresponding miR-379KO-HFD mice (Figures 4K and 4L). Binding of VEGFB to its receptor VEGFR1/Flt1 activates the VEGF/VEGFR2 pathway and promotes angiogenesis, leading to increased capillary density and enhanced adipose tissue function.[22] The decreased expression of *Flt1* observed in gWAT from WT-HFD mice was significantly reversed in miR-379KO-HFD mice (Figures 4M and 4N).

Using IHC, we observed lower EDEM3 integrated density (InDen) in gWAT of WT-HFD-M and -F mice versus the respective Cons, which was restored in part in miR-379KO-HFD (M and F) mice (Figures 5A, 5D, and 5E). VEGFB InDen was also significantly lower in gWAT of WT-HFD (M and F) mice compared with miR-379KO-HFD mice (Figures 5B, 5F, and 5G). Angiogenesis is reduced in inflamed adipose tissue.[23] To determine the functional outcome of altered VEGFB levels, gWAT tissue sections were stained for CD31, an endothelial cell marker, and for Perilipin, a cell surface marker of adipocytes (Figure 5C). Quantitative analysis showed significant reduction in capillary density (angiogenesis) and CD31 expression in gWAT from WT-HFD mice, and these aberrant changes were reversed in miR-379KO-HFD mice (Figures 5H and 5I).

HFD-induced expression of inflammatory genes in gWAT of WT-HFD mice is reduced in miR-379KO-HFD mice

We next assessed the expression of proinflammatory genes associated with IR, including interleukin 1 beta (*Il-1β*), and monocyte chemoattractant protein 1 (*Mcp-1/Ccl2*) in gWAT samples. *Il-1β* levels were significantly increased in gWAT from WT-HFD-M and -F mice but not in miR-379KO-HFD mice (M and F). *Mcp-1* levels were significantly increased in gWAT from WT-HFD-M and -F mice and in miR-379KO-HFD-M mice but not in miR-379KO-HFD-F mice (Figures 6A–6D). Quantitative analyses of immunofluorescence (IF) images showed that levels of F4/80, a marker of macrophage infiltration and inflammation, were increased in gWAT from WT-HFD mice but markedly attenuated in miR-379KO-HFD mice (M and F). Macrophage infiltration appeared to be generally lower in females than males on the HFD (Figures 6E–6G). The extracellular matrix (ECM) accumulation detected by periodic acid-Schiff (PAS) staining that was clearly increased in WT-HFD mice was attenuated in miR-379KO-HFD mice (M and F) (Figure 6H). These data demonstrate that obesity-induced increases in inflammation and ECM accumulation in gWAT during HFD are attenuated in miR-379KO mice with some sex differences.

Insulin signaling is attenuated in gWAT of miR-379KO-HFD mice relative to the corresponding WT-HFD mice

Insulin signaling via its receptor (insulin receptor [INSR]) and downstream AKT kinase regulates adipose metabolism, and this is downregulated during IR.[24] To determine the potential regulatory effect of miR-379 on insulin signaling in adipose tissue, we measured levels of p-AKT (phospho-S473) and p-INSR (phospho-Y1361) by IHC staining (Figures 6I–6N). We observed decreases in p-AKT levels in gWAT of WT-HFD-M mice compared with WT-Con but not in miR-379KO-HFD-M compared with the respective Con mice (Figure 6J). In F mice, levels of p-AKT were higher in miR-379KO-HFD-F mice relative to other groups (Figures 6I and 6K). We also observed decreases in p-INSR levels in gWAT of WT-HFD-M and -F mice compared with the respective Cons. Quantitative evaluations showed that these reductions were significantly attenuated in miR-379KO-HFD-M and -F mice compared with WT-HFD (M and F) mice (Figures 6L–6N).

These data show that parameters of IR are improved in gWAT of miR-379KO mice and more so in F mice than M mice. This matches earlier data showing that the improvements in ITT and IR as well as inflammation in gWAT are more pronounced in F miR-379KO-HFD mice than M mice, revealing sex-specific differences. On the other hand, improvements in parameters of BAT function were similar in M and F miR-379KO-HFD mice relative to WT-HFD mice.

Figure 3. Lack of miR-379 promotes mitochondrial function markers in BAT

(A) H&E staining shows increased lipid droplets and whitening of brown adipose tissue (BAT) in M and F WT-HFD mice, which are reduced in miR-379KO-HFD mice. The arrow indicates lipid droplets in BAT. (B and C) IHC staining of (B) FIS1 and (C) UCP-1 in BAT in M and F mice. (D and E) Quantitative analysis of FIS1 expression in (D) M and (E) F mice after 24 weeks of HFD feeding. n = 20 areas/group. (F and G) Quantitative analysis of UCP-1 expression in (F) M and (G) F mice after 24 weeks of HFD feeding. n = 20 areas/group/M. n = 40 areas/group/F. Scale bars, 50 μm; 20× magnification. (H and I) *miR-379* gene expression in BAT of (H) M and (I) F mice. n = 5/group. (J and K) *Fis1* gene expression in (J) M and (K) F mice. (L and M) *Ucp-1* gene expression in (L) M and (M) F mice at 24 weeks of HFD feeding. n = 5–6/group. Each dot represents one mouse/group. One-way ANOVA with post hoc Tukey's test for multiple comparisons; ±SEM; *p < 0.05, ***p < 0.001, ****p < 0.0001.

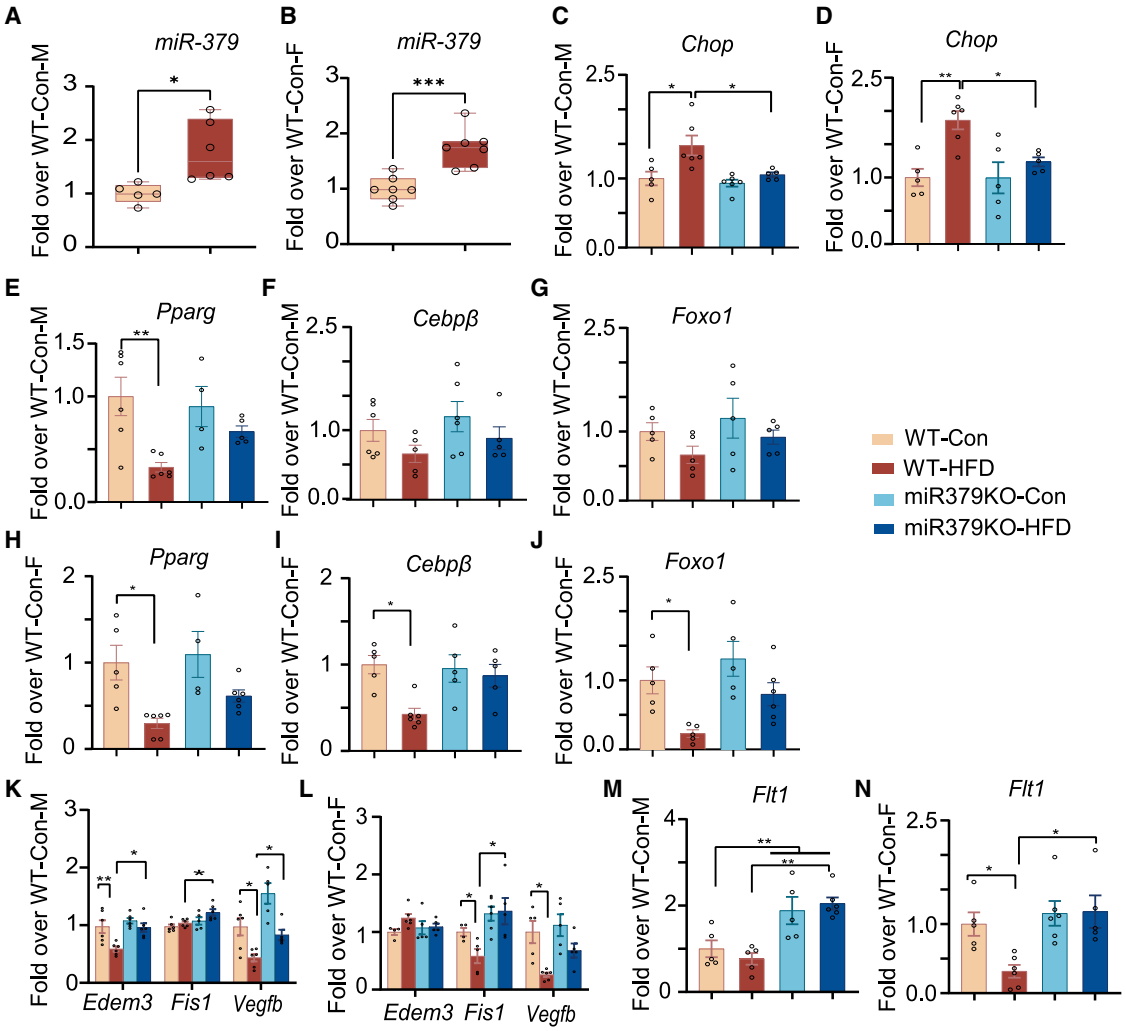

Figure 4. Increased expression of miR-379 and *Chop* and decreased expression of adipogenic markers in gWAT of WT-HFD mice are reversed in samples from miR-379KO-HFD mice

(A and B) miR-379 expression in (A) M and (B) F mice. n = 5–7/group. (C and D) *Chop* expression in (C) M and (D) F mice. n = 5–6/group. (E–J) expression of the adipogenesis-related genes *Pparg*, *Cebpβ*, and *Foxo1* in (E–G) M and (H–J) F mice in gWAT. n = 4–6/group. (K and L) Expression of miR-379 target genes (*Edem3*, *Fis1*, and *Vegfb*) in (K) M and (L) F mice. (M and N) Expression of *Flt1* (VEGF receptor 1) in (M) M and (N) F mice. 24 weeks of HFD experiments. n = 5–6/group. Each dot represents one mouse/group. One-way ANOVA with post hoc Tukey's test for multiple comparisons; ±SEM; *p < 0.05, **p < 0.01, ***p < 0.001.

miR-379 is increased in adipose tissue from obese individuals

The mouse miR-379 megacluster and lncMGC are located within the largest miRNA cluster identified in the *DLK-DIO3* genomic region (mouse chr12) and is conserved in the human genome (human chr14).[14] To demonstrate human relevance, we measured expression of miR-379 and several targets in WAT from lean, obese, and obese T2D individuals (obese/T2D). The clinical characteristics of the donors are described in Table S1. Relative to lean donors, obese and obese/T2D individuals had a significantly higher BMI (Figure 7A) and greater adipocyte hypertrophy in WAT samples (Figure 7B). miR-379 expression was significantly higher in WAT from obese and obese/T2D subjects (Figure 7C), and miR-379 expression in WAT positively correlated with BMI (Figure 7D).

miR-379 target genes are decreased in adipose tissue from obese individuals

We next examined the human adipose samples for expression of key miR-379 targets and related genes identified in mouse gWAT. We found that *EDEM3*, *VEGFB*, and *FLT1* were decreased in WAT from obese and obese/T2D individuals versus lean individuals (Figure 7E). We also found increased expression of *CHOP* and reduced expression of *PPARG* (Figures 7F and 7G). Expression of tumor necrosis factor alpha (*TNF-α*) (Figure 7H), which is augmented in hypertrophic and inflamed adipocytes and infiltrating macrophages,[25] was significantly increased in fat from obese and obese/T2D donors. IHC staining confirmed lower expression of VEGFB (Figures 7I and 7J) and VE-Cadherin (endothelial markers) (Figures 7I and 7K) in

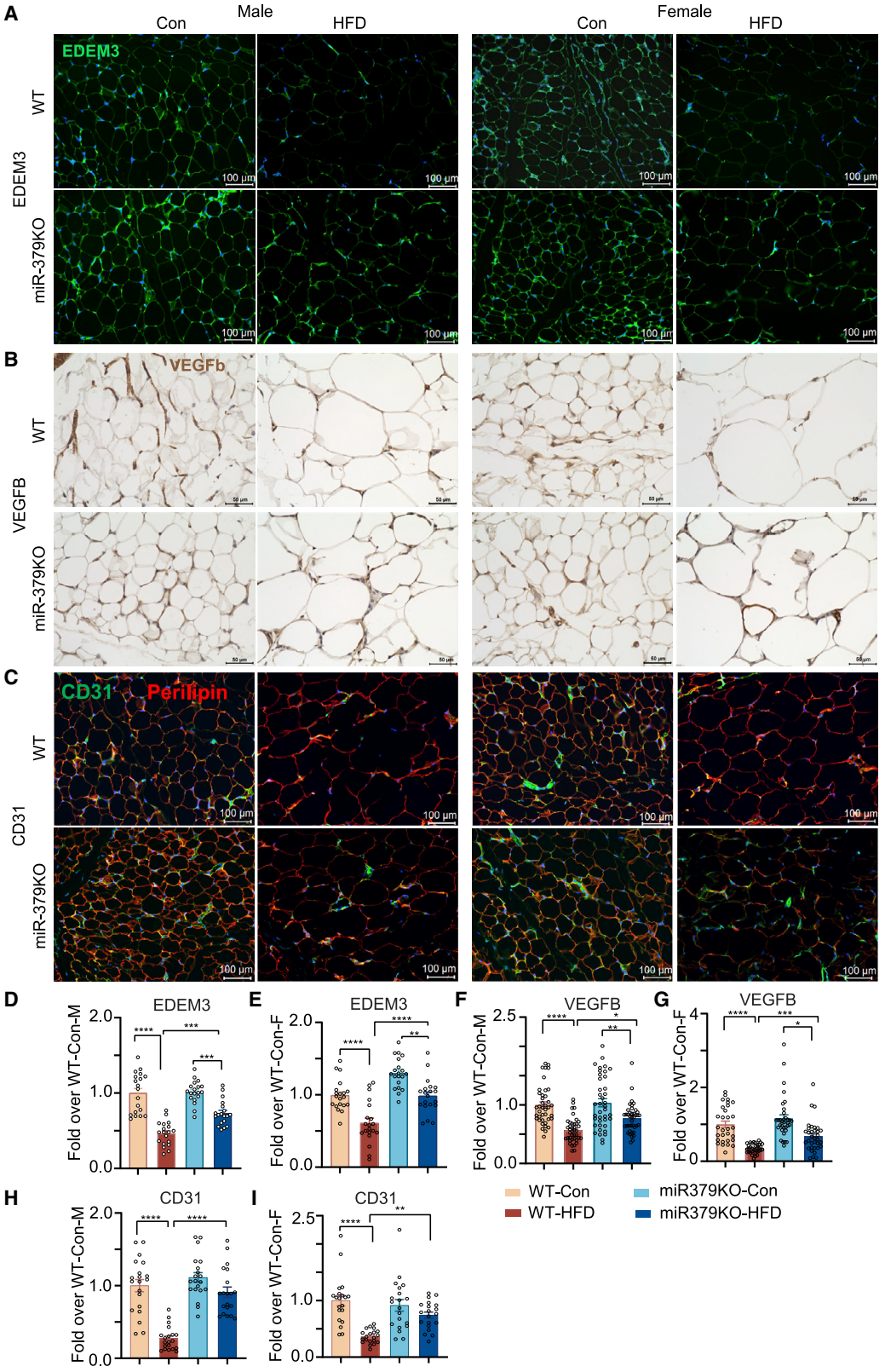

(legend on next page)

WAT from obese and obese/T2D donors. These data support the association of increased miR-379 and ER stress and decreased vascularization in fat tissue related to human obesity.

Alteration of miR-379 levels in mouse pre-adipocytes and differentiated adipocytes changes downstream gene expression

Mouse 3T3L1 pre-adipocytes were transfected with an miR-379 mimic oligonucleotide (oligo), miR-379 inhibitor oligo, or negative Con (NC) oligos for 24 h (Figures 8A–8H). Transfected cells were differentiated into adipocytes over 7 days using differentiation medium (Figures 8I–8R). Undifferentiated 3T3L1 pre-adipocytes were also treated with locked nucleic acid-modified antisense GapmeR oligos targeting miR-379 (miR-379-GapmeR) or NC GapmeR oligos for 4 days (Figures 8S–8X). miR-379 expression was significantly increased in cells transfected with miR-379 mimics and decreased in cells receiving the miR-379 inhibitor (Figures 8A, 8B, 8I, and 8J). Differentiated cells demonstrated lipid droplets (oil red O staining), which were significantly lower in cells transfected with miR-379 mimics (Figures 8K and 8L). 3T3L1 pre-adipocytes (Figures 8C and 8D) and differentiated adipocytes (Figures 8M and 8N) transfected with the miR-379 mimics showed decreased expression of the miR-379 target genes *Edem3* and *Vegfb*, which were restored by miR-379 inhibitors. GapmeR-mediated inhibition of miR-379 (Figure 8S) also upregulated the target genes (Figures 8T and 8U). *Chop* expression was decreased by a miR-379 inhibitor (Figures 8E and 8O) or miR-379-GapmeR (Figure 8V) relative to the respective NCs. Finally, we observed a significant increase in the adipogenic markers *Cebpβ*, *Foxo1*, and *Pparg* in pre-adipocytes (Figures 8F–8H) and in differentiated adipocytes (Figures 8P–8R) treated with a miR-379 inhibitor or miR-379-GapmeR (Figures 8W and 8X). These results suggest that miR-379 has a regulatory role in adipocyte differentiation, at least in part through modulating ER stress.

DISCUSSION

Our current results strongly indicate that upregulation of miR-379 plays an essential role in promoting gWAT and BAT dysfunction during obesity via downregulation of key miR-379 targets that have protective functions in adipose tissue. Our data demonstrate that miR-379 is upregulated in gWAT and BAT of WT-HFD-fed M and F mice and is associated with weight gain, adipocyte hypertrophy, hyperinsulinemia, and IR. These factors were significantly attenuated in miR-379KO-HFD mice, with some sex differences, with F miR-379KO-HFD mice showing relatively more protection from parameters of IR in gWAT relative to M mice. The decreased expression of mitochondrial function markers (FIS1, UCP-1, and PGC-1α) and mitochondrial damage in BAT of WT-HFD mice were restored or ameliorated in miR379KO-HFD mice (M and F), further supporting the involvement of miR-379 in pathologic processes related to adipose tissue dysfunction and obesity. The decreased expression of key miR-379 target genes with putative protective functions in adipose tissue (*Vegfb* and *Edem3*), increased expression of an ER stress marker (*Chop*) and proinflammatory genes (*IL-1β* and *Mcp-1*), and decreased expression of adipogenesis-related genes (*Pparg*, *Cebpβ*, and *Foxo1*) in gWAT in WT-HFD mice were reversed in miR-379KO-HFD mice with some sex differences. Our gain- and loss-of-function experiments in cultured adipocytes (3T3L1 cells) validated these target genes and provided mechanistic support for the regulatory effect of miR-379 on adipocyte differentiation. Similar to obese mice, we found increased expression of miR-379 in adipose tissue of obese individuals that positively correlated with their BMI. In parallel, we observed significant adipocyte hypertrophy and decreased vascularization and VEGFB expression along with increased *CHOP* and decreased *PPARG* expression in adipose tissue from obese individuals. Our finding that miR-379 expression is dysregulated in obesity is consistent with previous incidental findings showing that miR-379 is one of the miRNAs upregulated in adipose tissue[7] and liver in mouse models of obesity[26,27] as well as human donors with obesity.[27,28]

Adipose tissue expansion in obesity arises from adipocyte hypertrophy and/or hyperplasia as needed for increased lipid storage.[29] Adipocyte hypertrophy increases cellular stress; adverse metabolic profiles, including decreased insulin sensitivity; increased plasma insulin levels; and subsequent diabetes.[2] IR is a pathological feature of dysfunctional adipose tissue,[19] specifically visceral adipose tissue,[30] and increases during overnutrition. Several miRNAs have been shown to contribute to these pathologies.[31–35] Besides free fatty acids and various adipokines released from hypertrophic adipocytes, pro-inflammatory cytokines produced locally and from infiltrating macrophages promote inflammation and IR in obesity.[36] During HFD feeding, IR results from inhibition of insulin signaling via its insulin receptor and downstream IRS/Akt phosphorylation,[24] which also leads to impaired adipogenesis.[37,38] Our data suggest that miR-379 can have adverse effects of key factors related to insulin signaling in WAT and that miR-379 KO, especially in females, can attenuate these aberrant events.

Our results support involvement of miR-379 in pathologic processes related to obesity. Despite the similar effect of miR-379 deletion on reducing weight gain in M and F mice, we observed more significant improvements in whole-body IR and hyperinsulinemia in miR-379KO-HFD-F mice versus WT-HFD mice (Figures 1 and 2) relative to miR-379KO-HFD-M mice. This is consistent with our results showing that the decreases in macrophage

Figure 5. miR-379KO reverses HFD-mediated suppression of EDEM3 and the angiogenic markers VEGFB and CD31 in gWAT

(A–C) Immunofluorescence (IF) staining of EDEM3 (A), IHC staining of VEGFB (B), and IF staining of CD31 (C) in gWAT sections of M and F mice. (D and E) Quantitative analysis of EDEM3 in (D) M and (E) F mice. n = 20 areas/group. Scale bars, 100 μm. 20× magnification. Green, EDEM3. (F and G) Quantitative analysis of VEGFB in (F) M and (G) F mice. n = 40 areas/group. Scale bars, 50 μm. 40× magnification. (H and I) Quantitative analysis of CD31 in (H) M and (I) F mice. n = 20 areas/group. Scale bars, 100 μm. 20× magnification Green, CD31; red, Perilipin; blue, nucleus, DAPI. 24 weeks of HFD experiments. One-way ANOVA with post hoc Tukey's test for multiple comparisons, ±SEM; *p < 0.05, **p < 0.01, ***p < 0.001, ****p < 0.0001.

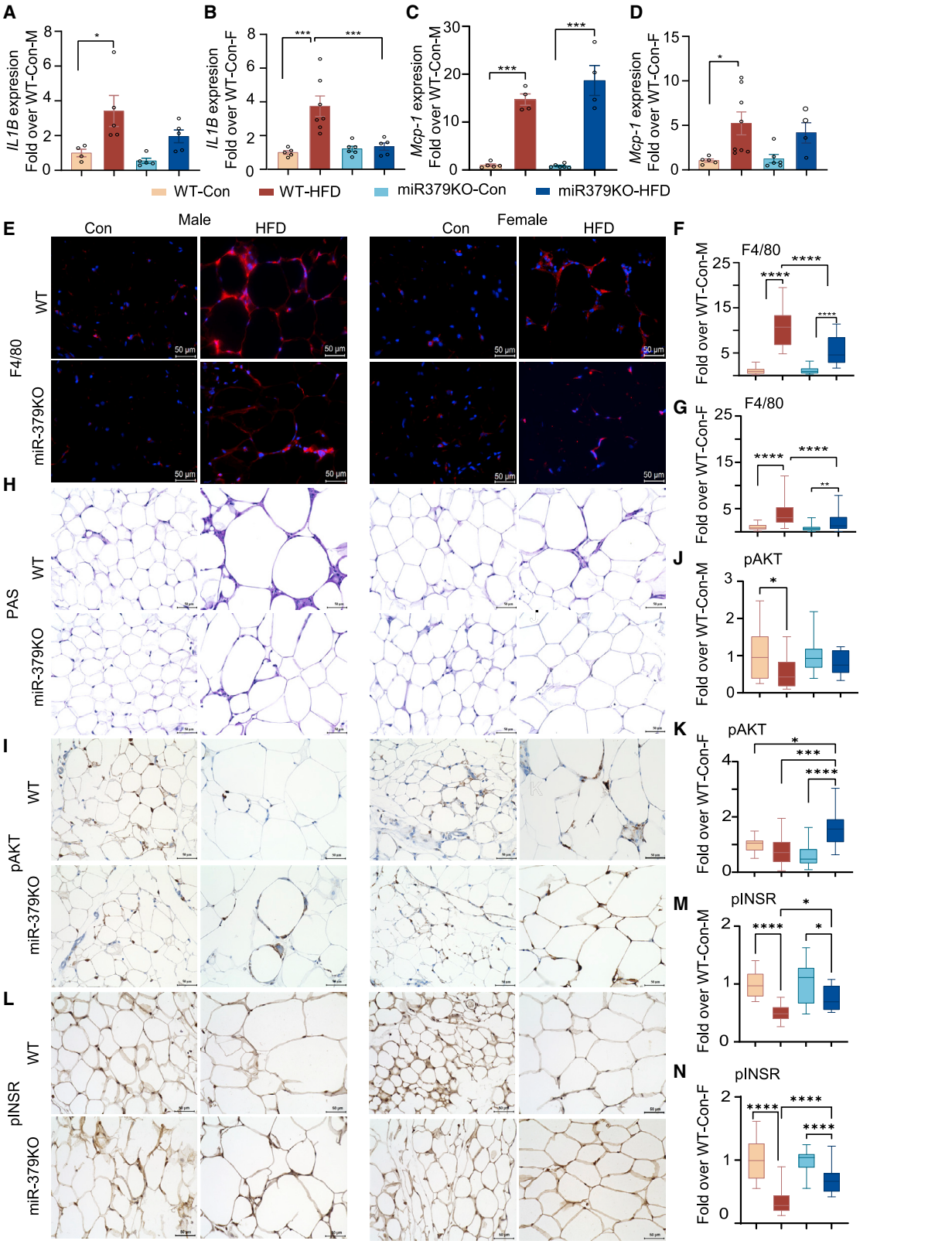

(legend on next page)

infiltration and parameters of IR in gWAT were more significantly ameliorated in miR-379KO-HFD-F mice relative to miR-379KO-HFD-M mice (Figure 6).

Therefore, in miR-379KO mice, improvements in BAT function may control obesity through mitochondrial functions regulated by miR-379, whereas changes in gWAT may control IR through targeting inflammation, ER stress, and insulin signaling regulated by miR-379. Thus, our data suggest that the obesogenic effect of miR-379 arises from its effects in BAT and gWAT (Figure S9). It is possible that parameters of IR and insulin signaling showed greater improvements in F miR-379KO-HFD mice relative to M mice because, overall, M mice showed greater increases in body weight as well as inflammation in gWAT. Because estrogen can decrease inflammation,[39] it could potentially be involved in protective effects and reduced inflammation in gWAT in miR-379KO-HFD-F mice.

ER stress in adipose tissue is increased during obesity and is strongly associated with chronic inflammation, IR, and T2D.[40] We previously identified *Edem3*, a negative regulator of ER stress, as one of the targets of miR-379 in the kidneys.[14,15] Here we found that HFD upregulated the ER stress-responsive marker *Chop* and downregulated *Edem3* in adipose tissue of obese human subjects versus lean subjects as well as in gWAT of WT-HFD versus miR-379KO-HFD mice. Because regulation by the ER stress-related TF CHOP is one mechanism by which miR-379 and the miR-379 cluster of miRNAs can be upregulated,[14] these data suggest that HFD increases *Chop* expression, which promotes ER stress and upregulation of miR-379 in gWAT. Deletion of miR-379 can thus reduce ER stress in a feedback manner by reducing *Chop* and subsequently decreasing miR-379 expression (Figure S9). This is consistent with reports showing upregulation of *Chop* in adipose tissue in the obese state.[41,42] CHOP can promote M1 polarization of adipose tissue macrophages to link ER stress with inflammation and IR.[41] *Chop* deficiency decreases adipose tissue inflammation and prevents IR[41] and inhibits downregulation of *Pparg*,[41,43] which is essential for adipogenesis and maintenance of the differentiated state.[19,30]

Using cultured 3T3L1 cells, we also demonstrated that miR-379 has a regulatory effect on adipogenesis. miR-379 mimics downregulated expression of key miR-379 targets as well as the adipogenic markers *Cebpβ* and *Pparg* compared with NC-treated cells. Conversely, miR379 inhibitor oligos increased expression of some of these adipogenic markers, including *Foxo1*. This is in line with reports showing that some miRNAs regulate adipogenesis by targeting PPARg or proteins involved in PPARg activity.[44] Other studies have shown decreased expression of adipose tissue *Pparg* in HFD-fed mice[19,33,45] and obese human individuals.[46] Adipogenesis is a complex process regulated directly or indirectly by several regulatory factors, including the C/EBPs and PPARg.[11,47] However, upregulation of anti-adipogenic TFs such as CHOP prevents activation of CEBPβ.[48] Interaction between CHOP and C/EBP modulates the transcriptional activity at CEBP-binding sites in the promoters of various genes important for maintaining the fat cell phenotype.[49] Foxo1, a member of the Forkhead TFs expressed in insulin-responsive tissues, is involved in adipocyte differentiation[50] and is regulated by ER stress.[51,52] Adipocyte differentiation is severely impaired in Foxo1-deficient 3T3L1 adipocytes, and downregulation of *Foxo1* decreases expression of *Pparg*.[21] Healthy expansion of adipose tissue is associated with proper angiogenesis regulated by a fine balance between actions of anti- and pro-angiogenic factors, such as VEGFs.[22] Persistent stress and long-term and severe hypoxia can impair angiogenesis and promote unhealthy adipose tissue expansion.[53] Our current results suggest that miR-379KO can also protect against HFD-induced gWAT dysfunction by increasing VEGFB and angiogenesis.

The protective phenotype observed in miR-379KO-HFD mice could be the cumulative effects of miR-379KO not only in adipose but also other insulin-sensitive tissues. However, we found that, relative to WT-HFD mice, our miR-379KO-HFD mice (M and F) also showed higher mitochondrial function (UCP-1, FIS1, and PGC-1) in BAT (Figures 3, S6, and S7), along with decreases in BAT whitening, suggesting that these effects in BAT may contribute to protection from HFD-induced weight gain. On the other hand, because miR-379KO females showed greater protection from IR in gWAT (likely dependent on ER stress) relative to males, it suggests distinct functions of miR-379 in BAT and gWAT with some sex differences. Our unpublished data showed attenuated lipid accumulation in the liver of miR-379KO-HFD mice relative to WT-HFD mice, but further studies are needed to systematically examine the involvement of miR-379 and its targets in the liver and other insulin-responsive tissues. miR-379 may also have additional effects via still unidentified targets in adipose and other tissue.

Our data implicate ER stress resulting from increased expression of miR-379 and concomitant reduction of its targets as key integrating mechanisms in HFD-induced adipose tissue inflammation and dysfunction, which involves a "feedback amplification loop" because of downregulation of *Edem3* and upregulation of *Chop*, which, in turn, amplifies ER stress (Figure S9).[14,15] Our data also suggest that increased miR-379 can promote BAT dysfunction via changes in mitochondria (Figure S9). Thus, inhibiting miR379 using modalities like GapmeRs can have beneficial effects on adipose dysfunction,

Figure 6. miR-379 regulates inflammatory gene expression and insulin signaling under HFD feeding

(A–D) Expression of *IL-1β* in gWAT in (A) M and (B) F mice and *Mcp-1* in (C) M and (D) F mice. n = 4–8/group. Each dot represents 1 mouse/group. (E) IF staining of F4/80 (red signals) in gWAT sections in M and F mice. (F and G) Quantitative analysis of F4/80 in (F) M and (G) F mice (n = 40–50 areas/group). (H) PAS (periodic acid-Schiff) staining in gWAT sections. 24 weeks of HFD experiments. Scale bars, 50 μm; 40× magnification. (I–N) miR-379 plays a role in HFD-mediated suppression of insulin signaling in gWAT. (I) Levels of p-AKT in M and F mice. (J and K) Quantitative analysis of pAKT in (J) M and (K) F mice. n = 15 area/group. (M and N) Quantitative analysis of p-INSR in (M) M and (N) F mice after 24 weeks of HFD feeding. n = 20–30 areas/group. Scale bars, 50 μm; 40× magnification. One-way ANOVA with post hoc Tukey's test for multiple comparisons ±SEM; *$p < 0.05$, **$p < 0.01$, ***$p < 0.001$, ****$p < 0.0001$.

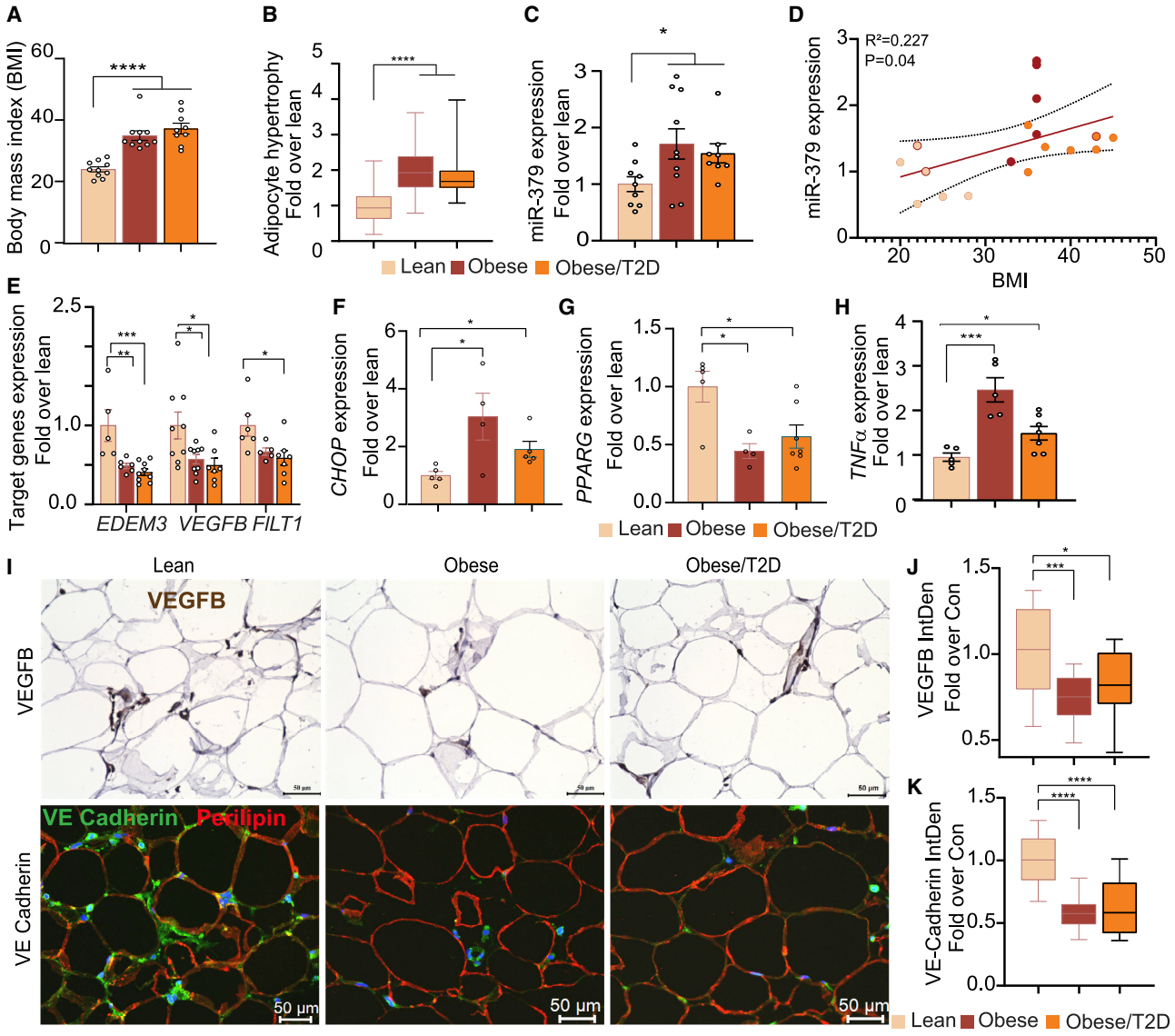

Figure 7. miR-379 is increased, and key targets of miR-379 are decreased, in adipose tissue from obese human subjects

(A) Body mass index (BMI) in lean, obese, and obese individuals with T2D (obese/T2D). n = 10–11/group. (B) Quantitative analysis of adipocyte size (n = 100 adipocytes/group). (C) Adipose tissue miR-379 expression (n = 8–10/group). (D) Correlation of miR-379 gene expression with BMI (n = 18). (E) Expression of target genes in adipose tissue from lean, obese, and obese/T2D donors. (F–H) adipose tissue gene expression of (F) *CHOP*, (G) *PPARG*, and (H) *TNF-α*. n = 4–7/group. (I) IHC staining of VEGFB (scale bars, 50 μm; 40× magnification) and IF staining of VE-Cadherin in adipose tissue from lean, obese, and obese/T2D donors. Scale bars, 50 μm; 40× magnification. Green, VE-Cadherin; red, Perilipin; blue, nucleus, DAPI. (J and K) Quantitative analysis of (J) VEGFB (n = 20–30 areas/group) and (K) VE-Cadherin (n = 20 areas/group). Data were analyzed using Student's t tests for comparisons between two groups. ±SEM; *p < 0.05, **p < 0.01, ***p < 0.001, ****p < 0.0001.

obesity, and obesity-associated comorbidities, including T2D, with therapeutic implications because miRNA inhibitors are already in clinical trials for various human disorders.[54]

MATERIALS AND METHODS

Mouse model of obesity and metabolic parameters

All animal studies were conducted according to protocols approved by the Institutional Animal Care and Use Committee at the Beckman Research Institute of City of Hope. We used homozygous *miR-379*$^{-/-}$ (miR-379KO) mice generated by CRISPR-Cas9 editing as reported by us.[15] Eight-week-old M and F C57BL/6J WT mice and miR-379KO mice were randomly divided into groups and fed a Con chow diet or HFD (60% kcal from fat) (D12492I, Research Diets) for 10 and 24 weeks. Body weight and BGLs were measured weekly. After euthanasia, plasma was collected to measure insulin, and gWAT and BAT were harvested (Figure S1).

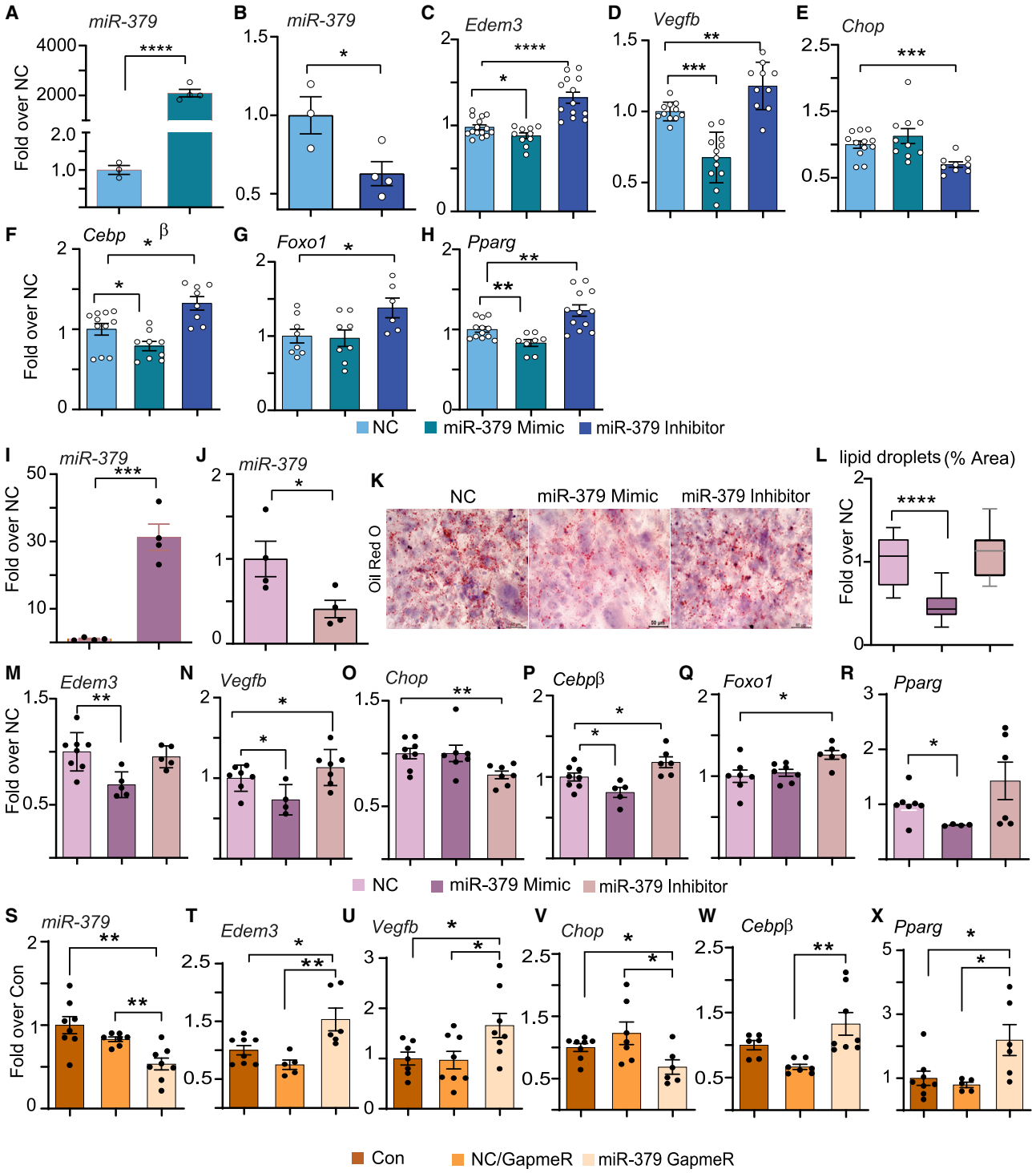

Figure 8. miR-379 regulates key factors related to adipogenesis in 3T3L1 adipocytes

3T3L1 pre-adipocytes were transfected with the miR-379 mimic oligo and miR-379 inhibitor (200 nmol/L). Cells transfected with negative Con (NC) oligos (200 nmol/L) were used as NCs. (A) miR-379 expression in cells transfected with the miR-379 mimic oligo. (B) miR-379 expression in cells transfected with the miR-379 inhibitor. n = 3–4/group. (C and D) Expression of the miR-379 target genes (C) *Edem3* and (D) *Vegfb*. (E–H) Expression of (E) *Chop* and the adipogenesis-related genes (F) *Cebpβ*, (G) *Foxo1*, and (H) *Pparg*. n = 8–12/group. (I–R) 3T3L1 pre-adipocytes were transfected with miR-379 mimic or miR-379 inhibitor oligos or NC. (I) miR-379 expression in miR-379 mimic-treated cells. (J) miR-379 expression in miR-379 inhibitor-transfected cells. n = 4/group. (K) Differentiation was confirmed using oil red O staining. Cells transfected with NC oligos

(legend continued on next page)

For ITTs, mice were fasted 2 h[55] and then injected intraperitoneally with 0.5 U insulin/kg body weight. BGLs were measured at 15, 30, 60, 90, and 120 min. The AUC was calculated with GraphPad Prism software. Plasma insulin levels were measured using a mouse ELISA kit (Crystal Chem, 90080). HOMA-IR was calculated according to the following formula: fasting insulin (μU/L) × fasting glucose (nmol/L)/22.5.[56] Body composition and metabolic parameters were measured in the City of Hope Comprehensive Metabolic Phenotyping core as described previously.[15] Whole-body composition was determined using quantitative magnetic resonance imaging (EchoMRI 3-in-1; Echo Medical Systems, Houston, TX). Body composition and metabolic parameters, such as energy expenditure, food intake, water consumption, and locomotor activity, were measured using an indirect calorimetry cage system (PhenoMaster, TSE Systems, Bad Homburg, Germany), as described previously.[15] Energy intake per mouse was calculated using the following equation as described previously:[57] kcal = food intake (g) × diet energy (kcal/g) (standard chow diet, 3.80 kcal/g; HFD, 5.34 kcal/g).

Human adipose tissue samples

We received discard de-identified human visceral adipose tissue from the Southern California Islet Cell Resource Center (City of Hope) for use in obesity- and diabetes-related research. The study was approved as exempt by the City of Hope institutional review board. Visceral WAT was divided into 3 categories (lean, obese, and obese/T2D) based on the donor's BMI and hemoglobin A1c (HbA1c) (Table S1).

Quantitative reverse transcriptase polymerase chain reaction

Quantitative reverse transcriptase polymerase chain reaction (qRT-PCR) analysis was performed as described previously.[14,15] mRNA expression was normalized to *Cypa* as an internal Con. For miRNAs, the universal primer was used as the reverse primer and U6 as an internal Con (Quanta Biosciences, Gaithersburg, MD).[15] PCR primer sequences are shown in Table S2.

Histology and IHC analysis

Paraffin-embedded gWAT sections were used for routine histology. Deparaffinized tissue slides were stained with H&E for morphological structure and PAS stain for ECM. Adipocyte size was assessed using light microscopy and quantified through Image-Pro Premier 9.2 software.

Antibodies targeting the proteins EDEM3 (1:100, NBP1-88342, Novus Biologicals, Centennial, CO, USA), VEGFB (1:200, MAB751, R&D Systems, Minneapolis, MN), UCP-1 (1:1,000, ab10983, Abcam, Waltham, MA), p-AKT (1:50, 4060, Cell Signaling Technology), and p-INSR (1:50, ab60946, Abcam) were used in IHC. Biotinylated goat anti-rabbit (1:400, BA-1000, Invitrogen) was used as a secondary antibody. Images were taken at 20× magnification, and InDen was quantified using ImageJ software.

Antibodies for other proteins characterized by specific IF included anti-F4/80 (1:200, 14-4801-82, Invitrogen), anti-EDEM3 (1:100, NBP1-88342, Novus Biologicals), anti-CD31 (1:20, ab28364, Abcam), anti-VE-Cadherin (1:150, ab33168, Abcam), and anti-Perilipin (1:300, 20R-PP004, Fitzgerald Industries). Secondary antibodies employed were Alexa Fluor 488, goat anti-rabbit (1:400, A11034, Invitrogen), and Alexa Fluor 555, goat anti-mouse (1:400, A21422, Invitrogen). Images were taken at 20× magnification (KEYENCE-BZ-×800 series, Osaka, Japan), and fluorescence intensity was measured using ImageJ software (ImageJ.win32).

TEM

BAT was collected from WT and miR-379KO HFD-fed mice, fixed in 2.5% (v/v) glutaraldehyde solution, and processed for TEM examination according to routine TEM processing and staining protocols for tissue in the City of Hope Electron Microscopy and Atomic Force Microscopy Core. TEM was performed on an FEI Tecnai 12 transmission electron microscope equipped with a Gatan Ultrascan 2 K charge-coupled device (CCD) camera.[14,15]

Cell transfection

Oligo mimics and inhibitors of miR-379 (200 nmol/L) and the corresponding Con oligos (NC) (200 nmol/L) were from Integrated DNA Technologies (IDT) or Thermo Fisher Scientific (Waltham, MA). 3T3L1 cells (~10^6/transfection) were transfected with these oligos using an Amaxa Nucleofector (Program A-033, Lonza, VPI-1004, Switzerland), as described previously.[15,58] Cells were collected 1 day after transfection or left for differentiation before RNA extraction.

Cell differentiation

3T3L1 pre-adipocytes were cultured in DMEM with 10% (v/v) bovine calf serum. Differentiation into adipocytes was promoted by culturing cells in differentiation medium (90% DMEM, 10% fetal bovine serum,1.0 μmol/L dexamethasone, 0.5 mmol/L methylisobutylxanthine, 5.0 μg/mL insulin) for 48 h. After 2 days, the medium was replaced with adipocyte maintenance medium (90% DMEM, 10% bovine calf serum, 5.0 μg/mL insulin), which was changed every 48 h until the cells were differentiated at ~7 days. The presence of lipid droplets in mature adipocytes was confirmed using 0.5% oil red O. Briefly, the cells were fixed with 10% formalin for 10 min, then changed to 2 mL fresh formalin, and incubated for 1 h. After rinsing with double-distilled water (ddH_2O) and 60% isopropanol (5 min), the cells were stained with oil red O (10 min) (Sigma, O-0625). Excess stain was removed by washing 4

(200 nmol/L) were used as NCs. (L) Percentage of oil red O-positive area (n = 20 area/group). (M and N) Expression of the miR-379 target genes (M) *Edem3* and (N) *Vegfb*. (O–R) Expression of (O) *Chop* and the adipogenesis-related genes (P) *Cebpβ*, (Q) *Foxo1*, and (R) *Pparg*. n = 4–8/group. (S–X) 3T3L1 pre-adipocytes were transfected with NC GapmeR or miR-379-GapmeR (1 μmol/L) as described under materials and methods. Non-transfected cells were used as a Con. (S) miR-379 expression (n = 8/group). (T and U) Expression of the miR-379 target genes (T) *Edem3* and (U) *Vegfb*. (V–X) Expression of (V) *Chop* and the adipogenic related genes (W) *Cebpβ* and (X) *Pparg*. n = 6–8/group. Data were analyzed using Student's t tests for comparisons between two groups. ±SEM; *p < 0.05, **p < 0.01, ***p < 0.001, ****p < 0.0001.

times with ddH_2O, and then cells were counterstained with hematoxylin.

GapmeR targeting miR-379

Locked nucleic acid (LNA)-modified GapmeRs (DNA-LNA chimeric antisense oligos) were optimized,[14,59] and the most effective GapmeR sequence, (379F [full 21-mer 5′-CCTacgttccatagtctaCCA-3']; LNA [uppercase], DNA [lowercase], phosphorothioate [PS; backbone]) from IDT was used. 3T3L1 pre-adipocytes were transfected with 1 μmol/L miR-379-GapmeR or NC GapmeR (5′-ATTttattcggaGCT-3′ LNA [uppercase], DNA [lowercase], PS [backbone]) for 4 days by Gymnosis[60] and cultured in 12-well plates. Untreated cells were used as Cons.[58]

Statistics

Animal cohorts consisted of 5–12 mice/group. Power calculations to estimate the sample size showed that eight animals per group would yield 80% power to detect a mean difference of 1.5 SD (effect size, 1.5) with two-tailed tests at a significance level of $p < 0.05$. *In vitro* experiments were performed at least three times. Data were analyzed with GraphPad Prism software, using Student's t tests for comparisons between two groups or two-way repeated-measures ANOVA or one-way ANOVA with post hoc tests for multiple groups.

AVAILABILITY OF DATA AND MATERIAL

The primary data for this study are available from the authors upon request.

SUPPLEMENTAL INFORMATION

Supplemental information can be found online at https://doi.org/10.1016/j.omtn.2022.09.015.

ACKNOWLEDGMENTS

We are grateful to members of the Natarajan laboratory for helpful discussions and to Dr. Jeffrey Isenberg (Arthur Riggs Diabetes and Metabolism Research Institute) for assistance with the manuscript. These studies were supported by grants from the National Institutes of Health (NIH) (R01 DK081705, R01 DK065073, and R01 HL106089 to R.N.) and a postdoctoral fellowship from the Larry L. Hillblom Foundation (to R.T.). Research reported in this publication also included work performed in the following Cores: Pathology Research Services, Light Microscopy/Digital Imaging Core, Electron Microscopy (EM/AFM) Core, and Comprehensive Metabolic Phenotyping, supported by the National Cancer Institute of the NIH under award P30CA33572 as well as the Animal Resource Center and Transgenic/Knockout Animal Cores at City of Hope.

AUTHOR CONTRIBUTIONS

M.A., M.K., and R.N. designed research. M.A., M.K., L.L., R.T., Y.W and M.W. performed research. M.A analyzed the data and generated all figures and tables. M.A., M.K., and R.N. wrote and edited the manuscript. Q.W., W.H., and P.T.F. provided valuable advice and edited the manuscript. All authors have read and approved the manuscript.

DECLARATION OF INTERESTS

The authors declare no competing interests.

REFERENCES

1. Sarma, S., Sockalingam, S., and Dash, S. (2021). Obesity as a multisystem disease: trends in obesity rates and obesity-related complications. Diabetes Obes. Metab. *23*, 3–16.
2. Rosen, E.D., and Spiegelman, B.M. (2014). What we talk about when we talk about fat. Cell *156*, 20–44.
3. Wozniak, S.E., Gee, L.L., Wachtel, M.S., and Frezza, E.E. (2009). Adipose tissue: the new endocrine organ? A review article. Dig. Dis. Sci. *54*, 1847–1856.
4. Jin, H., Li, D., Wang, X., Jia, J., Chen, Y., Yao, Y., Zhao, C., Lu, X., Zhang, S., Togo, J., et al. (2018). VEGF and VEGFB play balancing roles in adipose differentiation, gene expression, and function. Endocrinology *159*, 2036–2049.
5. Kusminski, C.M., Bickel, P.E., and Scherer, P.E. (2016). Targeting adipose tissue in the treatment of obesity-associated diabetes. Nat. Rev. Drug Discov. *15*, 639–660.
6. Banerjee, A., Sharma, D., Trivedi, R., and Singh, J. (2020). Treatment of insulin resistance in obesity-associated type 2 diabetes mellitus through adiponectin gene therapy. Int. J. Pharm. *583*, 119357.
7. Li, P., Chen, X., Chang, X., Tang, T., and Qi, K. (2020). A preliminary study on the differential expression of long noncoding RNAs and messenger RNAs in obese and control mice. J. Cell. Biochem. *121*, 1126–1143.
8. Kato, M., and Natarajan, R. (2019). Epigenetics and epigenomics in diabetic kidney disease and metabolic memory. Nat. Rev. Nephrol. *15*, 327–345.
9. Tanwar, V.S., Reddy, M.A., and Natarajan, R. (2021). Emerging role of long non-coding RNAs in diabetic vascular complications. Front. Endocrinol. *12*, 665811.
10. Das, S., Reddy, M.A., Senapati, P., Stapleton, K., Lanting, L., Wang, M., Amaram, V., Ganguly, R., Zhang, L., Devaraj, S., et al. (2018). Diabetes mellitus-induced long noncoding RNA Dnm3os regulates macrophage functions and inflammation via nuclear mechanisms. Arterioscler. Thromb. Vasc. Biol. *38*, 1806–1820.
11. Sun, L., and Lin, J.D. (2019). Function and mechanism of long noncoding RNAs in adipocyte biology. Diabetes *68*, 887–896.
12. Das, S., Zhang, E., Senapati, P., Amaram, V., Reddy, M.A., Stapleton, K., Leung, A., Lanting, L., Wang, M., Chen, Z., et al. (2018). A novel angiotensin II-induced long noncoding RNA giver regulates oxidative stress, inflammation, and proliferation in vascular smooth muscle cells. Circ. Res. *123*, 1298–1312.
13. Kato, M., and Natarajan, R. (2015). MicroRNAs in diabetic nephropathy: functions, biomarkers, and therapeutic targets. Ann. N. Y. Acad. Sci. *1353*, 72–88.
14. Kato, M., Wang, M., Chen, Z., Bhatt, K., Oh, H.J., Lanting, L., Deshpande, S., Jia, Y., Lai, J.Y.C., O'Connor, C.L., et al. (2016). An endoplasmic reticulum stress-regulated lncRNA hosting a microRNA megacluster induces early features of diabetic nephropathy. Nat. Commun. *7*, 12864.
15. Kato, M., Abdollahi, M., Tunduguru, R., Tsark, W., Chen, Z., Wu, X., Wang, J., Chen, Z.B., Lin, F.M., Lanting, L., et al. (2021). miR-379 deletion ameliorates features of diabetic kidney disease by enhancing adaptive mitophagy via FIS1. Commun. Biol. *4*, 175.
16. Longo, M., Zatterale, F., Naderi, J., Parrillo, L., Formisano, P., Raciti, G.A., Beguinot, F., and Miele, C. (2019). Adipose tissue dysfunction as determinant of obesity-associated metabolic complications. Int. J. Mol. Sci. *20*, E2358.
17. Song, A., Dai, W., Jang, M.J., Medrano, L., Li, Z., Zhao, H., Shao, M., Tan, J., Li, A., Ning, T., et al. (2020). Low- and high-thermogenic brown adipocyte subpopulations coexist in murine adipose tissue. J. Clin. Invest. *130*, 247–257.
18. Ikeda, K., and Yamada, T. (2020). UCP1 dependent and independent thermogenesis in Brown and beige adipocytes. Front. Endocrinol. *11*, 498.
19. (2020). Adipocytes fail to maintain cellular identity during obesity due to reduced PPARγ activity and elevated TGFβ-SMAD signaling. H.C. Roh, M. Kumari, S. Taleb, D. Tenen, C. Jacobs, A. Lyubetskaya, L.T. Tsai, and Rosen., eds. *42*, 101086.
20. Guo, S. (2014). Insulin signaling, resistance, and the metabolic syndrome: insights from mouse models into disease mechanisms. J. Endocrinol. *220*. T1–t23.
21. Munekata, K., and Sakamoto, K. (2009). Forkhead transcription factor Foxo1 is essential for adipocyte differentiation. In Vitro Cell. Dev. Biol. Anim. *45*, 642–651.

22. Robciuc, M.R., Kivelä, R., Williams, I.M., de Boer, J.F., van Dijk, T.H., Elamaa, H., Tigistu-Sahle, F., Molotkov, D., Leppänen, V.M., Käkelä, R., et al. (2016). VEGFB/VEGFR1-Induced expansion of adipose vasculature counteracts obesity and related metabolic complications. Cell Metab. *23*, 712–724.

23. Nijhawans, P., Behl, T., and Bhardwaj, S. (2020). Angiogenesis in obesity. Biomed. Pharmacother. *126*, 110103.

24. Li, H., Yu, L., and Zhao, C. (2019). Dioscin attenuates high-fat diet-induced insulin resistance of adipose tissue through the IRS-1/PI3K/Akt signaling pathway. Mol. Med. Rep. *19*, 1230–1237.

25. Stapleton, K., Das, S., Reddy, M.A., Leung, A., Amaram, V., Lanting, L., Chen, Z., Zhang, L., Palanivel, R., Deiuliis, J.A., and Natarajan, R. (2020). Novel long noncoding RNA, macrophage inflammation-suppressing transcript (MIST), regulates macrophage activation during obesity. Arterioscler. Thromb. Vasc. Biol. *40*, 914–928.

26. Cao, C., Duan, P., Li, W., Guo, Y., Zhang, J., Gui, Y., and Yuan, S. (2021). Lack of miR-379/miR-544 cluster resists high-fat diet-induced obesity and prevents hepatic triglyceride accumulation in mice. Front. Cell Dev. Biol. *9*, 720900.

27. de Guia, R.M., Rose, A.J., Sommerfeld, A., Seibert, O., Strzoda, D., Zota, A., Feuchter, Y., Krones-Herzig, A., Sijmonsma, T., Kirilov, M., et al. (2015). microRNA-379 couples glucocorticoid hormones to dysfunctional lipid homeostasis. EMBO J. *34*, 344–360.

28. Okamoto, K., Koda, M., Okamoto, T., Onoyama, T., Miyoshi, K., Kishina, M., Matono, T., Kato, J., Tokunaga, S., Sugihara, T., et al. (2020). Serum miR-379 expression is related to the development and progression of hypercholesterolemia in non-alcoholic fatty liver disease. PLoS One *15*, e0219412.

29. Wang, Q.A., Tao, C., Gupta, R.K., and Scherer, P.E. (2013). Tracking adipogenesis during white adipose tissue development, expansion and regeneration. Nat. Med. *19*, 1338–1344.

30. Rosen, E.D., and MacDougald, O.A. (2006). Adipocyte differentiation from the inside out. Nat. Rev. Mol. Cell Biol. *7*, 885–896.

31. Chakraborty, C., Doss, C.G.P., Bandyopadhyay, S., and Agoramoorthy, G. (2014). Influence of miRNA in insulin signaling pathway and insulin resistance: micro-molecules with a major role in type-2 diabetes. Wiley Interdiscip. Rev. RNA *5*, 697–712.

32. Zhang, F., Ma, D., Zhao, W., Wang, D., Liu, T., Liu, Y., Yang, Y., Liu, Y., Mu, J., Li, B., et al. (2020). Obesity-induced overexpression of miR-802 impairs insulin transcription and secretion. Nat. Commun. *11*, 1822.

33. Srivastava, A., Shankar, K., Beg, M., Rajan, S., Gupta, A., Varshney, S., Kumar, D., Gupta, S., Mishra, R.K., and Gaikwad, A.N. (2018). Chronic hyperinsulinemia induced miR-27b is linked to adipocyte insulin resistance by targeting insulin receptor. J. Mol. Med. *96*, 315–331.

34. Kurylowicz, A. (2021). microRNAs in human adipose tissue physiology and dysfunction. Cells *10*, 3342.

35. Trajkovski, M., Hausser, J., Soutschek, J., Bhat, B., Akin, A., Zavolan, M., Heim, M.H., and Stoffel, M. (2011). MicroRNAs 103 and 107 regulate insulin sensitivity. Nature *474*, 649–653.

36. Kang, Y.E., Kim, J.M., Joung, K.H., Lee, J.H., You, B.R., Choi, M.J., Ryu, M.J., Ko, Y.B., Lee, M.A., Lee, J., et al. (2016). The roles of adipokines, proinflammatory cytokines, and adipose tissue macrophages in obesity-associated insulin resistance in modest obesity and early metabolic dysfunction. PLoS One *11*, e0154003.

37. Cignarelli, A., Genchi, V.A., Perrini, S., Natalicchio, A., Laviola, L., and Giorgino, F. (2019). Insulin and insulin receptors in adipose tissue development. Int. J. Mol. Sci. *20*, E759.

38. Barilla, S., Treuter, E., and Venteclef, N. (2021). Transcriptional and epigenetic control of adipocyte remodeling during obesity. Obesity *29*, 2013–2025.

39. Louet, J.-F., LeMay, C., and Mauvais-Jarvis, F. (2004). Antidiabetic actions of estrogen: insight from human and genetic mouse models. Curr. Atheroscler. Rep. *6*, 180–185.

40. Reilly, S.M., and Saltiel, A.R. (2017). Adapting to obesity with adipose tissue inflammation. Nat. Rev. Endocrinol. *13*, 633–643.

41. Suzuki, T., Gao, J., Ishigaki, Y., Kondo, K., Sawada, S., Izumi, T., Uno, K., Kaneko, K., Tsukita, S., Takahashi, K., et al. (2017). ER stress protein CHOP mediates insulin resistance by modulating adipose tissue macrophage polarity. Cell Rep. *18*, 2045–2057.

42. Chen, Y., Wu, Z., Zhao, S., and Xiang, R. (2016). Chemical chaperones reduce ER stress and adipose tissue inflammation in high fat diet-induced mouse model of obesity. Sci. Rep. *6*, 27486.

43. Maris, M., Overbergh, L., Gysemans, C., Waget, A., Cardozo, A.K., Verdrengh, E., Cunha, J.P.M., Gotoh, T., Cnop, M., Eizirik, D.L., et al. (2012). Deletion of C/EBP homologous protein (Chop) in C57Bl/6 mice dissociates obesity from insulin resistance. Diabetologia *55*, 1167–1178.

44. Zhang, M., Zhou, Z., Wang, J., and Li, S. (2016). MiR-130b promotes obesity associated adipose tissue inflammation and insulin resistance in diabetes mice through alleviating M2 macrophage polarization via repression of PPAR-γ. Immunol. Lett. *180*, 1–8.

45. Nakae, J., Kitamura, T., Kitamura, Y., Biggs, W.H., 3rd, Arden, K.C., and Accili, D. (2003). The forkhead transcription factor Foxo1 regulates adipocyte differentiation. Dev. Cell *4*, 119–129.

46. Hammes, T.O., Costa, C.d.S., Rohden, F., Margis, R., de Almeida, J.C., Padoin, A.V., Mottin, C.C., and Guaragna, R.M. (2012). Parallel down-regulation of FOXO1, PPARγ and adiponectin mRNA expression in visceral adipose tissue of class III obese individuals. Obes. Facts *5*, 452–459.

47. Wang, Q.A., Tao, C., Jiang, L., Shao, M., Ye, R., Zhu, Y., Gordillo, R., Ali, A., Lian, Y., Holland, W.L., et al. (2015). Distinct regulatory mechanisms governing embryonic versus adult adipocyte maturation. Nat. Cell Biol. *17*, 1099–1111.

48. Tang, Q.Q., and Lane, M.D. (2000). Role of C/EBP homologous protein (CHOP-10) in the programmed activation of CCAAT/enhancer-binding protein-beta during adipogenesis. Proc. Natl. Acad. Sci. USA *97*, 12446–12450.

49. Ron, D., and Habener, J.F. (1992). CHOP, a novel developmentally regulated nuclear protein that dimerizes with transcription factors C/EBP and LAP and functions as a dominant-negative inhibitor of gene transcription. Genes Dev. *6*, 439–453.

50. Chen, J., Lu, Y., Tian, M., and Huang, Q. (2019). Molecular mechanisms of FOXO1 in adipocyte differentiation. J. Mol. Endocrinol. *62*. R239–r253.

51. Zhou, Y., Lee, J., Reno, C.M., Sun, C., Park, S.W., Chung, J., Lee, J., Fisher, S.J., White, M.F., Biddinger, S.B., and Ozcan, U. (2011). Regulation of glucose homeostasis through a XBP-1-FoxO1 interaction. Nat. Med. *17*, 356–365.

52. Chipurupalli, S., Samavedam, U., and Robinson, N. (2021). Crosstalk between ER stress, autophagy and inflammation. Front. Med. *8*, 758311.

53. Halberg, N., Khan, T., Trujillo, M.E., Wernstedt-Asterholm, I., Attie, A.D., Sherwani, S., Wang, Z.V., Landskroner-Eiger, S., Dineen, S., Magalang, U.J., et al. (2009). Hypoxia-inducible factor 1alpha induces fibrosis and insulin resistance in white adipose tissue. Mol. Cell Biol. *29*, 4467–4483.

54. Chakraborty, C., Sharma, A.R., Sharma, G., and Lee, S.S. (2021). Therapeutic advances of miRNAs: a preclinical and clinical update. J. Adv. Res. *28*, 127–138.

55. Moro, C., and Magnan, C. (2021). GTTs and ITTs: aim for shorter fasting times. Nat. Metab. *3*, 1133.

56. Fraulob, J.C., Ogg-Diamantino, R., Fernandes-Santos, C., Aguila, M.B., and Mandarim-de-Lacerda, C.A. (2010). A mouse model of metabolic syndrome: insulin resistance, fatty liver and non-alcoholic fatty pancreas disease (NAFPD) in C57BL/6 mice fed a high fat diet. J. Clin. Biochem. Nutr. *46*, 212–223.

57. Vinolo, M.A.R., Rodrigues, H.G., Festuccia, W.T., Crisma, A.R., Alves, V.S., Martins, A.R., Amaral, C.L., Fiamoncini, J., Hirabara, S.M., Sato, F.T., et al. (2012). Tributyrin attenuates obesity-associated inflammation and insulin resistance in high-fat-fed mice. Am. J. Physiol. Endocrinol. Metab. *303*, E272–E282.

58. Kato, M., Putta, S., Wang, M., Yuan, H., Lanting, L., Nair, I., Gunn, A., Nakagawa, Y., Shimano, H., Todorov, I., et al. (2009). TGF-beta activates Akt kinase through a microRNA-dependent amplifying circuit targeting PTEN. Nat. Cell Biol. *11*, 881–889.

59. Putta, S., Lanting, L., Sun, G., Lawson, G., Kato, M., and Natarajan, R. (2012). Inhibiting microRNA-192 ameliorates renal fibrosis in diabetic nephropathy. J. Am. Soc. Nephrol. *23*, 458–469.

60. Stein, C.A., Hansen, J.B., Lai, J., Wu, S., Voskresenskiy, A., Høg, A., Worm, J., Hedtjärn, M., Souleimanian, N., Miller, P., et al. (2010). Efficient gene silencing by delivery of locked nucleic acid antisense oligonucleotides, unassisted by transfection reagents. Nucleic Acids Res. *38*, e3.